BRAIN
A JOURNAL OF NEUROLOGY

Inhibiting poly(ADP-ribose) polymerase: a potential therapy against oligodendrocyte death

Sara Veto,[1,*] Peter Acs,[2,*] Jan Bauer,[3] Hans Lassmann,[3] Zoltan Berente,[1] Gyorgy Setalo Jr,[4] Gabor Borgulya,[5] Balazs Sumegi,[1] Samuel Komoly,[2] Ferenc Gallyas Jr[1] and Zsolt Illes[2]

1 Department of Biochemistry and Medical Chemistry, University of Pecs Medical School, Pecs, Hungary
2 Department of Neurology, University of Pecs Medical School, Pecs, Hungary
3 Centre for Brain Research, Medical University of Vienna, Austria
4 Department of Medical Biology, University of Pecs Medical School, Pecs, Hungary
5 3rd Department of Internal Medicine, Semmelweis University of Budapest, Budapest, Hungary

*These authors contributed equally to this work.

Correspondence to: Ferenc Gallyas Jr,
Department of Biochemistry and Medical Chemistry,
University of Pecs Medical School,
Pecs, 12 Szigeti St,
Hungary
E-mail: ferenc.gallyas@aok.pte.hu

Oligodendrocyte loss and demyelination are major pathological hallmarks of multiple sclerosis. In pattern III lesions, inflammation is minor in the early stages, and oligodendrocyte apoptosis prevails, which appears to be mediated at least in part through mitochondrial injury. Here, we demonstrate poly(ADP-ribose) polymerase activation and apoptosis inducing factor nuclear translocation within apoptotic oligodendrocytes in such multiple sclerosis lesions. The same morphological and molecular pathology was observed in an experimental model of primary demyelination, induced by the mitochondrial toxin cuprizone. Inhibition of poly(ADP-ribose) polymerase in this model attenuated oligodendrocyte depletion and decreased demyelination. Poly(ADP-ribose) polymerase inhibition suppressed c-Jun N-terminal kinase and p38 mitogen-activated protein kinase phosphorylation, increased the activation of the cytoprotective phosphatidylinositol-3 kinase-Akt pathway and prevented caspase-independent apoptosis inducing factor-mediated apoptosis. Our data indicate that poly(ADP-ribose) polymerase activation plays a crucial role in the pathogenesis of pattern III multiple sclerosis lesions. Since poly(ADP-ribose) polymerase inhibition was also effective in the inflammatory model of multiple sclerosis, it may target all subtypes of multiple sclerosis, either by preventing oligodendrocyte death or attenuating inflammation.

Introduction

Multiple sclerosis is a chronic disease of the central nervous system that is characterized by a presumed autoimmune inflammation, demyelination and axonal degeneration (Noseworthy *et al.*, 2000). Although immunomodulatory treatments are available to counteract the common inflammatory pathology, no treatments exist to prevent demyelination, which may contribute to axonal degeneration, the best pathological correlate of clinical disability in multiple sclerosis (Naismith and Cross, 2005).

While destruction of myelin develops in association with inflammation, in the earliest lesions of pathological subtypes for patterns III and IV, apoptosis-like depletion of oligodendrocytes has been described, suggesting degenerative processes (Lucchinetti *et al.*, 2000). An alternative hypothesis to the heterogeneous pathogenesis of multiple sclerosis even proposes that oligodendrocyte apoptosis represents the first and earliest stage of all lesions, resulting in primary demyelination that unmasks tissue antigens and secondary autoimmune inflammation (Barnett and Prineas, 2004). Depletion of oligodendrocytes then occurs progressively during lesion evolution (Frohman *et al.*, 2006).

Recently, mitochondrial dysfunction has been suggested to play a role in the loss of oligodendrocytes and axons in multiple sclerosis (Kalman *et al.*, 2007). Fulminate multiple sclerosis lesions with profound oligodendrocyte apoptosis (pattern III) reveal a pattern of hypoxia-like tissue injury, which seems to be induced by a dysfunction in complex IV of the respiratory chain (Lucchinetti *et al.*, 2000; Aboul-Enein *et al.*, 2003; Mahad *et al.*, 2008). In such multiple sclerosis lesions, oligodendrocyte apoptosis follows a caspase-independent pathway (Aboul-Enein *et al.*, 2003; Barnett and Prineas, 2004).

A non-inflammatory experimental primary demyelination, induced by a copper chelator cuprizone in weanling mice, results in multi-focal demyelination and loss of oligodendrocytes in particular brain areas, mainly the corpus callosum and superior cerebellar peduncle (Matsushima and Morell, 2001). A mitochondrial aetiology was assumed since giant mitochondria have been observed in the liver of cuprizone-treated mice (Suzuki, 1969). Supporting this notion, increased production of reactive oxygen species and decreased activity of various complexes of the respiratory chain were found in the mitochondria of cuprizone-treated oligodendroglia cells (Pasquini *et al.*, 2007). However, and in contrast to experimental autoimmune encephalomyelitis, the number of T cells is negligible in the demyelinated corpus callosum and T cell activation has not been observed in the cuprizone model (Remington *et al.*, 2007).

Impaired functioning of the mitochondrial respiratory chain results in excessive production of reactive oxygen species, which cause damage to various cellular components including DNA (Turrens, 2003). The nuclear enzyme poly(ADP-ribose) polymerase (PARP) functions as a DNA damage sensor and signalling molecule, which forms long branches of ADP-ribose polymers on a number of nuclear target proteins, including itself (Alano *et al.*, 2004). Extensive DNA damage triggers overactivation of PARP, eventually resulting in cell dysfunction and death (Alano *et al.*, 2004).

Additionally, PARP activity appears to be essential for the mitochondria-to-nucleus translocation of apoptosis-inducing factor (AIF), supporting the hypothesis that nuclear mitochondrial crosstalk dependent on poly(ADP-ribosyl)ation is critical in determining the fate of injured cells (Yu *et al.*, 2002). This crosstalk is supposed to involve a PARP-dependent activation of c-Jun N-terminal kinase (JNK) and the cytoprotective phosphoinositol-3 kinase-Akt pathway (Tapodi *et al.*, 2005; Xu *et al.*, 2006). Furthermore, PARP has been shown to function as a co-activator in the nuclear factor-κB-mediated transcription, regulating the expression of various pro-inflammatory proteins (Oliver *et al.*, 1999).

PARP-mediated cell death and inflammation has been implicated in the pathogenesis of several central nervous system diseases (Kauppinen and Swanson, 2007). Inhibition of PARP activity reduced brain injury in ischaemia reperfusion and excitotoxicity (Endres *et al.*, 1997; Mandir *et al.*, 2000). It was also able to ameliorate inflammation in experimental autoimmune encephalomyelitis, the autoimmune model of multiple sclerosis (Scott *et al.*, 2004).

Considering similar observations suggesting mitochondrial pathology and sparse inflammation in both the cuprizone model and pattern III multiple sclerosis (Lucchinetti *et al.*, 2000; Aboul-Enein *et al.*, 2003; Pasquini *et al.*, 2007; Mahad *et al.*, 2008), the focus of this study was (i) to reveal PARP activation in multiple sclerosis plaques and the cuprizone-mediated non-inflammatory primary demyelination model of multiple sclerosis; (ii) to determine whether the inhibition of PARP could exert a protective effect against experimental demyelination; and (iii) to determine the underlying mechanisms.

Materials and methods

Cuprizone model and the administration of PARP inhibitor

C57BL/6 male mice were purchased from Charles River Laboratories Magyarorszag Kft (Isaszeg, Hungary) and kept under standardized, specific pathogen-free circumstances. Starting at 8 weeks of age, mice received a diet of powdered rodent chow containing 0.2% cuprizone (bis-cyclohexanone oxaldihydrazone) (Sigma, Steinheim, Germany) by weight for 3, 5 and 6 weeks *ad libitum* to induce demyelination, as described previously (Hiremath *et al.*, 1998). The PARP inhibitor 4-hydroxyquinazoline (4HQ, Sigma-Aldrich, Steinheim, Germany) (Banasik *et al.*, 1992) was administered i.p. at a dose of 100 mg/kg body mass and a volume of 10 μl/g body mass every day (Veres *et al.*, 2004), starting on the same day as the cuprizone treatment. Control mice received the same volume (10 μl/g) of saline solution instead of 4HQ. In order to follow the systemic effect of cuprizone, the weights' of the mice were measured every week (Hiremath *et al.*, 1998).

All animal experiments were carried out under legislation [1998/XXVIII Act of the Hungarian Parliament on Animal Protection and Consideration and Decree in Scientific Procedures of Animal Experiments (243/1998)] in laboratories in the University of Pecs. Licensing of procedures was controlled by The Committee on Animal

Research of the University of Pecs according to the Ethical Codex of Animal Experiments.

MRI and quantitative neuroimaging

At the beginning of treatment, and from the third week, mice were anaesthetized weekly by intraperitoneal injection of diazepam (5 mg/kg) and ketamine (80 mg/kg) (both purchased from Gedeon Richter Plc, Budapest, Hungary). The animals were then secured in an epoxy resin animal holder tube (Doty Scientific Inc., Columbia, SC, USA) custom modified to accommodate the tip of teeth and position the eyes of each animal in the same location -5.0 ± 0.5 mm above the isocentre of the magnet. A glass capillary filled with water:glycerol = 9:1 mixture was placed near the head of the animal, serving as an external signal intensity reference. Magnetic resonance images were obtained exactly as described before (Veres *et al.*, 2003, 2004). The extent of demyelination in the corpus callosum was determined by calculating the mean signal intensity of the corpus callosum divided by the mean signal intensity of the reference capillary. The mean signal intensities were determined by freehand delineation of regions of interest in the corpus callosum or the reference capillary on coronal cross-sectional images exactly 1 mm posterior from the bregma by an investigator blind to the experiment.

Histopathology

After 5 weeks of treatment mice were terminally anaesthetized with intraperitoneally administered diazepam and ketamine and perfused via the left ventricle with 4% paraformaldehyde in a phosphate buffer containing picric acid. After overnight postfixation in the same fixative, brains were dissected. Brains were embedded in paraffin before histological analysis, and then 8 µm coronal sections were obtained at the level of 161, 181, 209 and 221 (Sidman, 1971). Demyelination was evaluated using luxol fast blue staining with cresyl violet. Scoring on a scale of 0–3 was performed by three independent experts in a double-blind manner. A score of 3 was equivalent to the myelin status of a mouse not treated with cuprizone, whereas 0 was equivalent to totally demyelinated corpus callosum. A score of 1 and 2 indicates that one-third and two-thirds of the fibres of the corpus callosum were myelinated, respectively (Hiremath *et al.*, 1998). The mean scores of coronal sections of the corpus callosum from four different regions stained with luxol fast blue-cresyl violet were generated and the averages scores were used for statistical analysis.

Immunocytochemistry and confocal laser fluorescence microscopy for poly(ADP-ribose) and apoptosis-inducing factor in multiple sclerosis lesions

Poly(ADP-ribose) and AIF expression was studied in the lesions of 13 patients with multiple sclerosis and 5 control cases without neurological disease or brain lesions. The multiple sclerosis sample contained six cases with acute multiple sclerosis (Marburg, 1906), one case with relapsing remitting multiple sclerosis and six cases with chronic progressive multiple sclerosis (Table 1).

Lesion areas within the sections were defined according to activity: early pattern III lesions showed loss of myelin-associated glycoprotein (MAG), oligodendrocyte apoptosis and predominant infiltration by activated microglia; late active/inactive lesions in pattern III multiple sclerosis cases were densely infiltrated by macrophages with a variable content of myelin degradation products; normal appearing white matter areas were at least 1 cm apart from the active lesions.

In pattern II lesions, early stages revealed scattered infiltration of the tissue with macrophages and activated microglia; myelin sheaths were still present, but showed signs of acute dissolution. In late active/inactive pattern II lesions, myelin was completely lost and macrophages contained myelin degradation products at various stages of chemical myelin disintegration. The lesions in patients with progressive multiple sclerosis were slowly expanding lesions with a small rim of active demyelination (early lesions) with microglia activation and some macrophages containing the earliest stages of myelin degradation. The late active/inactive lesion centres were completely demyelinated and contained a variable, but generally low amount of macrophages with myelin degradation products.

Active lesions following pattern III (Lucchinetti *et al.*, 2000) were seen in four cases with acute multiple sclerosis, pattern II lesions were analysed in two cases of acute multiple sclerosis and one case with relapsing–remitting multiple sclerosis, and slowly expanding active lesions were present in six cases with progressive multiple sclerosis (Kutzelnigg *et al.*, 2005).

Immunocytochemistry was performed on paraffin sections as described before (Marik *et al.*, 2007) without antigen retrieval. Poly(ADP-ribose) antibody was purchased from Alexis Biotechnology, London, UK, and the AIF antibody from Chemikon International. For lesion characterization we used immunocytochemistry with antibodies against MAG, myelin oligodendrocyte glycoprotein, proteolipid protein, cyclic nucleotide phosphodiesterase and CD68, as described previously (Marik *et al.*, 2007).

Fluorescence immunohistochemistry was performed on paraffin sections as described earlier (Bauer *et al.*, 2007) with some modifications. Staining with primary antibody poly(ADP-ribose) or AIF was done overnight. As a second step, sections were incubated with a secondary biotinylated-anti-mouse antibody (Amersham Pharmacia Biotech; 1:200). This was followed by antigen retrieval by 60 min incubation in a plastic coplin jar filled with citrate buffer (0.01 M, pH 6.0) in a household food steamer device (MultiGourmet FS 20, Braun, Kronberg/Taunus, Germany). This first staining was finished with application of streptavidin-Cy2 (Jackson ImmunoResearch, West Grove, PA; 1:75) for 1 h at room temperature. After washing in tris-buffered saline, the sections were incubated overnight with anti-carbonic anhydrase II (The Binding Site Ltd, Birmingham, UK, for detection of oligodendrocytes). This was followed by washing and incubation with secondary Cy3-conjugated antibodies donkey-anti-sheep or donkey-anti-rabbit (both 1:100, both Jackson Immuno Research). The staining was finished with 4′,6′-diamidino-2-phenylindole (DAPI) (Sigma) counterstain. Sections were examined using a confocal laser scan microscope (Leica SP5, Mannheim, Germany). Recordings for Cy2 (excited with the 488 nm laser) and Cy3 (excited with the 543 nm laser) were done simultaneously and followed by recording for DAPI with a 405 nm laser.

Quantification of cells with poly(ADP-ribose) and AIF immunoreactivity

Poly(ADP-ribose)-positive cells were defined as cells with strong poly(ADP-ribose) immunoreactivity within the nuclei as well as in the cytoplasm, including cell processes; in the majority of these cells,

Table 1 Clinical data for multiple sclerosis patients

Case	Multiple sclerosis type	Gender	Age (years)	Duration (months)	Initial/early	Late act/inactive
MS III A	AcMS	Male	45	0.2	2	1
MS III B	AcMS	Male	45	0.6	3	2
MS III C	AcMS	Male	35	1.5	5	4
MS III D	AcMS	Male	78	2	1	1
MS II A	AcMS	Male	52	1.5	4	4
MS II B	AcMS	Female	51	5	2	1
MS II C	RRMS	Female	57	156	2	3
Chr MS A	SPMS	Male	41	137	2 (SEL)	2
Chr MS B	SPMS	Male	56	372	1 (SEL)	2
Chr MS C	SPMS	Female	46	444	2 (SEL)	2
Chr MS D	PPMS	Male	67	87	1 (SEL)	1
Chr MS E	PPMS	Female	77	168	1 (SEL)	1
Chr MS F	PPMS	Female	71	264	2 (SEL)	3
Normal controls		3 Male/2 Female	36–74	0	0	0

MS III = multiple sclerosis patients with pattern III lesions; MS II = multiple sclerosis cases with pattern II lesions; Chr MS = multiple sclerosis cases with slowly expanding lesions of progressive multiple sclerosis; AcMS = acute multiple sclerosis; RRMS = relapsing/remitting multiple sclerosis; SPMS = secondary progressive multiple sclerosis; PPMS = primary progressive multiple sclerosis; Initial/early = lesions at the early active stage of demyelination (in pattern III lesions in areas of MAG loss); Late act/inact = late active or inactive lesions, still containing macrophages with degradation products of different stages of myelin digestion; SEL = slowly expanding lesions with a small rim of microglia activation and early myelin degradation products at the margin. The numbers in the last two columns represent the numbers of different lesion types contained in the sections.

poly(ADP-ribose)-positive nuclei appeared condensed and, in part, fragmented, suggesting apoptosis. In addition cytoplasmic poly(ADP-ribose) reactivity revealed signs of cell degeneration consistent with in part fragmented cell processes and cytoplasmic vacuolization (Fig. 1K, L, V, X and Y). For quantification of AIF expression only those cells were counted that showed unequivocal immunoreactivity within their nuclei (Fig. 1P, Q and W).

Cells were counted manually (HL) in each of the above-defined areas in seven microscopic fields of $0.27 \, mm^2$ each. The values given in Table 2 represent cells/mm^2.

Immunohistochemistry, immunofluorescence and confocal microscopy of cuprizone lesions

Formation of poly(ADP-ribose) was analysed in paraffin sections of cuprizone-treated mice as described above for the analysis of multiple sclerosis tissue.

For further characterization of the lesions, 8 μm-thick, gelatine-coated slides were rehydrated, heat-unmasked, blocked in a solution containing 2% normal horse serum and phosphate buffered saline and incubated overnight with the primary antibody diluted in blocking solution. Primary antibodies against myelin basic protein (MBP) (1:75, Novocastra Laboratories Ltd), poly(ADP-ribose) (1:100, Alexis Biotechnology) and AIF (1:100, Cell Signalling Technology) were used. Appropriate biotinylated secondary antibodies (1:200, Molecular Probes) and 3,3'-diaminobenzidine reaction were used for visualization. For immunofluorescent labelling, Alexa 488 goat anti-rabbit secondary antibody (1:200, Molecular Probes) was applied with DAPI counterstaining for visualization of nuclei (VECTASHIELD HardSet Mounting Medium with DAPI, Vector Laboratories).

Confocal images were collected using an Olympus Fluoview FV-1000 laser scanning confocal imaging system and an Olympus UPLSAPO 60 × oil immersion objective lens (numeric aperture 1, 35). Sections were viewed with an Olympus BX-50 microscope and photographed with a SPOT RT colour digital camera. Cell nuclei were counterstained with DAPI, the dye was excited at 405 nm and its emission was detected in the range of 425–475 nm. The specific immune signal was generated using Alexa 488 excited with a 488 nm laser beam and detected in the range of 500–600 nm. Scanning of images occurred in a sequential line mode using line Kalman integration count 4. The confocal aperture was set to 100 μm. Supplemented images represent areas of 52 398 × 52 398 μm at a resolution of 640 × 640 pixels. With the imaging conditions used, there was no detectable bleedthrough of fluorescence from one channel to the other when we studied single-labelled specimen.

Immunoblot analysis

Tissue samples were taken from animals killed after 3 or 5 weeks of treatment. Corpus callosum of the mice were carefully dissected and 25 mg of the tissue was homogenized in ice-cold 10 mM tris buffer, pH 7.4 [containing 0.5 mM sodium metavanadate, 1 mM ethylenediaminetetraacetic acid and protease inhibitor cocktail (1:200); all purchased from Sigma-Aldrich, Steinheim, Germany]. Homogenates (10 μg each) were loaded onto 10 and 12% sodium dodecyl sulphate polyacrylamide gels, electrophoresed and transferred to nitrocellulose membranes. The following antibodies were used: anti-MBP (1:1000) (Novocastra Laboratories Ltd, Newcastle upon Tyne, UK), anti-poly(ADP-ribose) (1:1000) (Alexis Biotechnology, London, UK), anti-AIF (1:330) (Santa Cruz Biotechnology, Santa Cruz, CA, USA), anti-phospho-Akt (Ser^{473}) (1:1000) (R&D Systems, Minneapolis, MN, USA), anti-caspase-3 (1:1000), anti-nonphosphorylated Akt/protein kinase B (1:1000), anti-extracellular signal-regulated kinase 1/2 (ERK1/2) (Thr^{183}/Tyr^{185}) (1:1000), anti-phospho JNK (Thr^{183}/Tyr^{185}) (1:1000), anti-caspase-3 (1:1000) (all from Cell Signalling Technology,
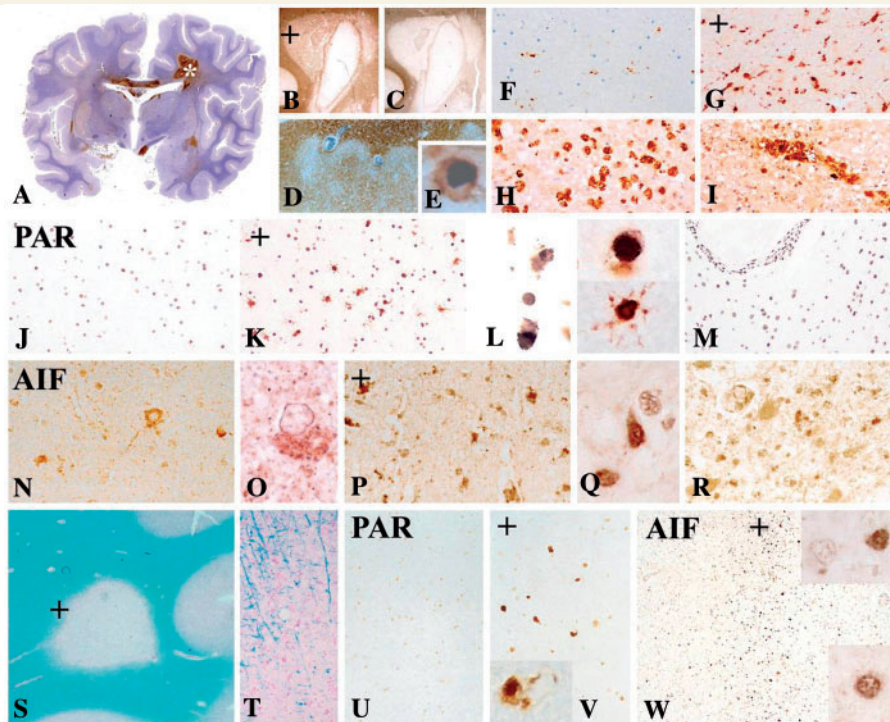
Figure 1 Activation of poly(ADP-ribose) polymerase (PAR) and nuclear translocation of AIF in different types of multiple sclerosis lesions. (**A–I**) Neuropathological characterization of multiple sclerosis pattern III lesions. (**A**) Hemispheric brain section of patient P III C, stained by immunocytochemistry for macrophages/microglia (CD68), shows multiple active lesions within the brain; the asterisk labels the lesion shown in Figs **B-L** (×0.3). Active pattern III lesion stained for myelin/oligodendrocyte glycoprotein (**B**) and MAG (**C**) showing loss of both myelin proteins in the centre of the lesion; in the very early lesion stages (+) MAG is completely lost from the lesion, while myelin/oligodendrocyte glycoprotein expression is partly preserved (×1.2). (**D**) Very early stage of pattern III lesion shows partial loss of myelin (stained for proteolipid protein), however, the inflamed vessels are surrounded by rim of preserved myelin (×40). (**E**) Within the active lesion oligodendrocytes that are stained for cyclic nucleotide phosphodiesterase show condensed nuclei reminiscent of apoptosis (×1200). Staining for CD68 shows only few activated microglia cells in the normal appearing white matter (**F**), a profound increase of activated microglia in early lesions showing selective loss of MAG (**G**); profound infiltration of the tissue with macrophages in late active portions of the lesion (**H**) and mainly perivascular accumulation of macrophages in the inactive lesion centre (**I**) (×200). Poly(ADP-ribose) expression in different lesion stages from the case shown in (**A–I**); in the normal appearing white matter (**J**) there is faint brown nuclear staining of glial cells; the nuclei are counterstained with haematoxylin (blue); in the area of MAG loss (the '+' indicates the location of the area in (**B**), numerous cells are seen with intense nuclear and cytoplasmic reactivity for poly(ADP-ribose) (**K**); higher magnification of the cells in (**L**), shows different examples of poly(ADP-ribose) positive glial cells with dark condensed nuclei and partial cytoplasmic or cell process dissolution; the lesion centre (**M**) shows weak brown immunoreactivity in some nuclei, similar to that seen in the normal-appearing white matter (×200; inserts ×1200). AIF expression in similar lesion areas of the same case shown for poly(ADP-ribose) before; (**N, O**) purely mitochondrial AIF expression in the normal appearing white matter; (**P, Q**): in the early active (MAG loss) lesions AIF is seen not only in mitochondria, but also in nuclei; (**R**) in the inactive lesion centre AIF is only present in mitochondria (×200; inserts ×1200). Poly(ADP-ribose) and AIF expression in a slowly expanding lesion in progressive multiple sclerosis (ChMS D); (**S**) shows the location of the lesion in the subcortical white matter (×4) and (**T**) documents the hypercellular margin of the lesions with some macrophages with recent myelin degradation products (×100); no poly(ADP-ribose) expression was seen in the normal appearing white matter (**U**); however, there is a moderate number of small oligodendrocyte like glia cells with strong poly(ADP-ribose) reactivity within condensed nuclei and cell processes (**V**); the + labels the active lesion area in (**S**), (**V**) and (**W**). (**W**) AIF expression is enriched in the area of active lesion expansion (+); in the majority of the cells AIF is seen as cytoplasmic granules, representing mitochondria (upper insert), but there is also AIF reactivity in nuclei of cells, resembling oligodendrocytes (lower insert) (×200).

Beverly, MA, USA), anti-phospho-p38-mitogen-activated protein kinase (MAPK) (Thr[180]/Tyr[182]) (1:1000) and anti-actin (1:10 000) (both from Sigma-Aldrich, Steinhein, Germany). Appropriate horseradish peroxidase-conjugated secondary antibodies were used at a 1:5000 dilution (anti-mouse and anti-rabbit IgGs; Sigma-Aldrich, Steinheim, Germany) and visualized by enhanced chemiluminescence (Amersham Biosciences, Piscataway, NJ, USA). Films were scanned and

the pixel volumes of the bands were determined using National Institutes of Health Image J software (Bethesda, MD, USA).

Caspase-3 activity assay

Carefully dissected corpus callosum samples (20 mg) from animals treated for 3 weeks were homogenized in the lysis buffer (50 mM

Table 2 Poly(ADP-ribose) and nuclear AIF expression in multiple sclerosis

Samples	MS III	MS II	Progressive	Controls
Cases	4	3	6	7
PAR early	71.4 ± 27.0***	1.6 ± 1.7	15.3 ± 9.2**	n.a.
PAR IA	22.2 ± 17.9**	0.2 ± 0.4	4.6 ± 7.3	n.a.
PAR NWM	5.0 ± 7.4	0.8 ± 0.7	1.4 ± 1.4	0.6 ± 0.7
AIF early	19.1 ± 7.7***	2.5 ± 2.8*	11.9 ± 5.0***	n.a.
AIF IA	9.0 ± 5.4**	2.5 ± 2.3	3.3 ± 3.8	n.a.
AIF NWM	4.9 ± 2.5***	1.0 ± 1.7	2.2 ± 2.6	0.2 ± 0.1

Quantitative analysis of cells with poly(ADP-ribose) immunoreactivity and nuclear AIF expression in glial cells in different types of multiple sclerosis lesions. The cases are identical to those described in Table 1; MS III = multiple sclerosis patients with pattern III lesions; MS II = multiple sclerosis cases with pattern II lesions; progressive = multiple sclerosis cases with slowly expanding lesions of progressive multiple sclerosis; PAR = poly(ADP-ribose); NWM = normal white matter. The numbers represent cells with positive immunoreactivity/mm². Mean ± SD in normal white matter, in early lesions of multiple sclerosis pattern III cases or at sites of initial myelin destruction in pattern II lesions or slowly expanding lesions in progressive multiple sclerosis (early), and in the centre of the lesions that still contained macrophages with myelin degradation products at different stages of digestion (IA). Significant difference from respective control normal white matter values was indicated $*P < 0.05$, $**P < 0.01$ and $***P < 0.001$.

Tris, pH 8) containing protease inhibitor cocktail (Sigma-Aldrich, Steinheim, Germany). Fluorometric assays were performed using fluorescent-labelled peptide substrate for caspase-3 (Ac-DEVD-AFC, Sigma-Aldrich, St Louis, MO, USA) and a fluorescence plate reader set at 360 nm excitation and 460 nm emission, as recommended by the manufacturer.

Statistics

The density of poly(ADP-ribose) and AIF-positive cells (Table 2) in each group of multiple sclerosis patients was compared with the respective values found in normal white matter of control brains using Scheffé's *post hoc* ANOVA test; heteroscedasticity was minimized with the logarithmic transformation. The repeated body weight measurements were analysed using a random intercept fixed slope linear model considering a common distribution of initial weights but separate slopes for the treatment groups. Relative corpus callosum MRI signal intensities in the treatment groups were compared with a mixed effect analysis of variance where individuals were modelled as random effects. The histological degrees of corpus callosum myelination were compared using the non-parametric Mann–Whitney test. The immunoblot band intensities in the four treatment groups were normalized to the loading control and compared pairwise using Scheffé's *post hoc* ANOVA test; heteroscedasticity was minimized with the logarithmic transformation. Differences were considered significant at values of $P < 0.05$ or lower.

Results

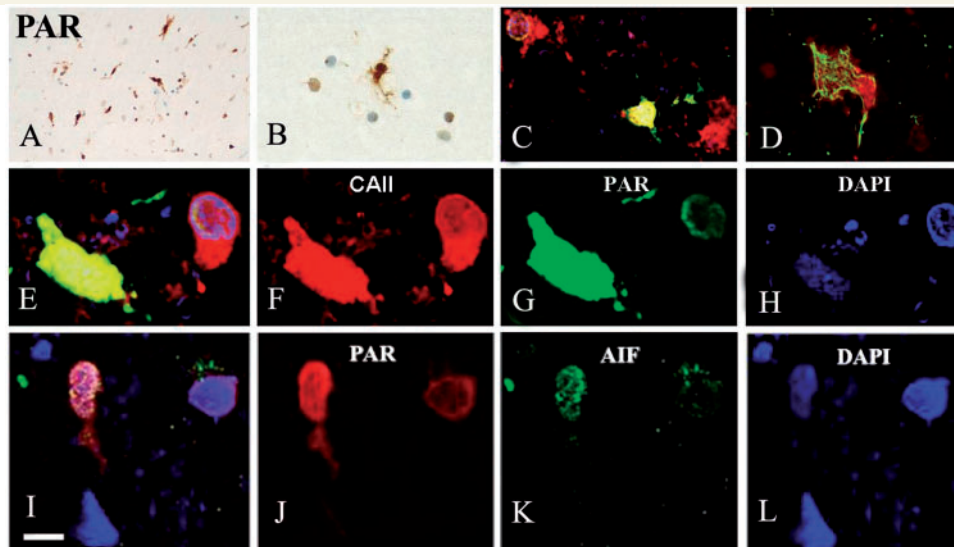## PARP activation in multiple sclerosis lesions and control brains

In order to determine PARP activation in multiple sclerosis lesions, we demonstrated accumulation of the enzyme's product by using anti-poly(ADP-ribose) immunofluorescence or immunohistochemistry. We observed very strong poly(ADP-ribose) reactivity in the nucleus and cytoplasm of single cells. This was most pronounced in patients with acute multiple sclerosis, in active lesions showing the characteristic pathological hallmarks of pattern III demyelination and containing high numbers of apoptotic oligodendrocytes, (Fig. 1A–I). The expression was seen in cells that, by the anatomy of their processes, mainly resembled oligodendrocytes (Fig. 1J–M and Fig. 2A and B). They contained a condensed, sometimes fragmented nucleus and their cytoplasm revealed, in part, fragmented cell processes or swelling and focal vacuoles (Fig. 1L). In addition, a few cells with astrocyte or macrophage morphology also showed strong poly(ADP-ribose) immunoreactivity. On the other hand, both multiple sclerosis and control tissue demonstrated weak-to-moderate labelling of nuclei for poly(ADP-ribose) (Fig. 1J and M). This was highly variable between cases, and independent of lesions in multiple sclerosis tissue. The observation of variable and moderate PARP activation in post-mortem tissues may reflect agonal events.

Quantitative analysis confirmed that poly(ADP-ribose) reactive glia cells were enriched in areas of initial and active myelin breakdown of pattern III lesions, as defined before (Marik *et al.*, 2007) (Table 2). Similar poly(ADP-ribose) reactive oligodendrocytes, although in lower numbers, were also seen at the active edge of slowly expanding lesions in progressive multiple sclerosis (Fig. 1S–V) and in lowest numbers in patients with pattern II lesions (Table 2). Double staining and confocal laser-scanning microscopy confirmed that the majority of cells with strong poly(ADP-ribose) immunoreactivity also expressed the oligodendrocyte marker carbonic anhydrase II (Fig. 2C, E–H), but that scattered cells also co-expressed poly(ADP-ribose) with either glial fibrillary acidic protein (Fig. 2D) or CD68 (data not shown). Poly(ADP-ribose) reactivity in oligodendrocytes exceeded that of astrocytes both in number of positive cells and intensity of the staining (Fig. 1K, L, V and Fig. 2A, B).

Nuclear translocation of AIF in pattern III multiple sclerosis lesions

Since AIF is essential in mediating PARP-dependent cell death (Yu *et al.*, 2002), we examined its expression in multiple sclerosis lesions. AIF reactivity in the normal brain, and with some exceptions in the normal appearing white matter of multiple sclerosis patients (Table 2), was confined to the mitochondria of neurons and glia cells (Fig. 1N, O). In multiple sclerosis lesions, AIF reactivity in mitochondria was enhanced (Fig. 1P–R, W) and seen not only in neurons and glia but also in macrophages. Within initial and active areas of multiple sclerosis pattern III lesions and much less in other active multiple sclerosis lesions (Table 2), we found a variable number of glia cells with nuclear AIF reactivity (Fig. 1P, Q and W) co-localized with increased anti-poly(ADP-ribose) staining in condensed nuclei, showing features of apoptosis (Fig. 2I–L). These data suggested that activation of PARP may result in AIF-mediated oligodendrocyte death in pattern III multiple sclerosis lesions.

Figure 2 Activation of poly(ADP-ribose) polymerase and nuclear translocation of AIF in active pattern III multiple sclerosis lesions. (**A–H**) show examples of poly(ADP-ribose) (PAR) reactivity within glial cells of an active pattern III lesions (within the area of MAG loss), showing by confocal microscopy double labelling for poly(ADP-ribose) (PAR) and carbonic anhydrase II (CAII) within an oligodendrocyte (**C**), for poly(ADP-ribose) and glial fibrillary acidic protein in an astrocyte (**D**) and triple labelling for carbonic anhydrase II (CAII; red; **F**), poly(ADP-ribose) (green; **G**) and DAPI (blue nuclei, **H**) in oligodendrocytes at different stages of degeneration; (**E**) shows the overlay of triple staining (×1200). (**J–L**) Representative confocal images of nuclear co-localization of poly(ADP-ribose) and AIF. poly(ADP-ribose) immunoreactivity (red), AIF immunoreactivity (green) and DAPI nuclear staining (blue) were presented individually and merged (**J**) (scale bar: 10 μm).

Cuprizone enhances PARP activation in the corpus callosum

In order to investigate the effect of PARP inhibition on experimental demyelination, we first examined the activation of PARP on cuprizone treatment. Cuprizone induced auto-poly(ADP-ribosyl)-ation, i.e. activation of PARP in corpus callosum of mice after 3 weeks of treatment ($P < 0.05$) (Fig. 3A). Expression of poly(ADP-ribose) immunoreactivity in the apoptotic nuclei of oligodendrocytes was confirmed by confocal laser microscopy (Fig. 3B and C). In addition, 4HQ—a potent inhibitor of the enzyme (Banasik *et al.*, 1992)—blocked both cuprizone induced and basal auto-poly(ADP-ribosyl)ation at a dose of 100 mg/kg used throughout this study ($P < 0.05$) (Fig. 3A). This dose of 4HQ was previously found to be effective and devoid of any apparent toxic effect (Veres *et al.*, 2004).

PARP inhibitor prevents weight loss, the systemic effect of cuprizone

Cuprizone caused weight loss in comparison to the control group ($P < 0.001$), which was effectively prevented by simultaneous administration of the PARP inhibitor ($P < 0.001$). 4HQ alone did not affect the growth rate ($P = 0.28$) (Fig. 4).

PARP inhibition protects against cuprizone-induced demyelination in the brain

Examination of the brain was performed by non-invasive *in vivo* MRI. In untreated mice, corpus callosum appeared hypointense on

T$_2$-weighted images. Upon cuprizone feeding, T$_2$-weighted images of corpus callosum showed hyperintensity corresponding to demyelination (Merkler *et al.*, 2005), which was most pronounced after 4 weeks. PARP inhibitor prevented cuprizone-induced hyperintensities in the corpus callosum (Fig. 5A).

Serial, quantitative neuroimaging indicated significant demyelination of the corpus callosum with cuprizone feeding after 3 weeks up to 6 weeks, which was most pronounced after 4 weeks of treatment and decreased thereafter. Inhibition of PARP prevented demyelination at all time points. When applied alone, 4HQ did not cause any changes in signal intensities (Fig. 5A).

Pathological analysis with luxol fast blue-cresyl violet staining revealed a profound demyelination in the corpus callosum of cuprizone-fed mice (Fig. 5B). According to a semi-quantitative histological analysis, 4HQ reduced the cuprizone-induced demyelination ($P < 0.001$) (data not shown). 4HQ alone did not affect myelination.

Quantitative MBP immunoblotting revealed decreased MBP expression after 5 weeks of cuprizone feeding ($P < 0.01$), which was reversed by the PARP inhibitor 4HQ ($P < 0.05$). The administration of the PARP inhibitor alone did not affect the MBP level (Fig. 5C). Similar results were found by MBP immunohistochemistry (data not shown).

Cuprizone induces caspase-independent AIF-mediated cell death, which is diminished by PARP-inhibition

Parallel to demyelination, we observed elevated expression of AIF in the corpus callosum of mice treated with cuprizone for 3 weeks,
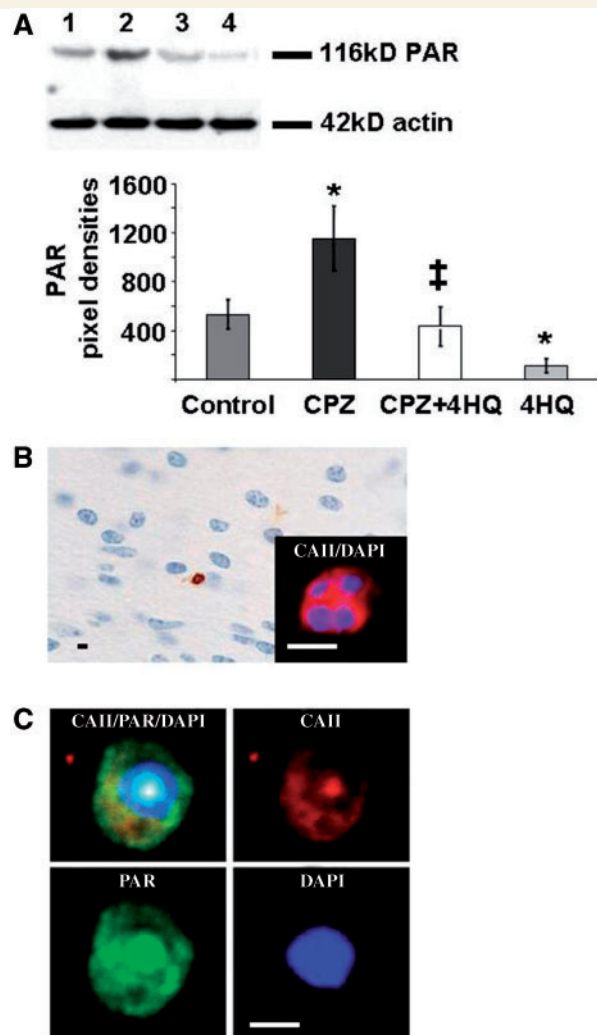
Figure 3 Effect of cuprizone and 4HQ treatment on poly(ADP-ribose) polymerase activation. (**A**) Representative immunoblots for PARP auto-ADP-ribosylation (upper panel) and their densitometric evaluation (lower panel). Auto-ADP-ribosylation of PARP in the dissected corpus callosum of mice treated for 3 weeks was detected by immunoblotting utilizing an anti-ADP-ribose antibody. Even protein loadings were confirmed by an anti-actin antibody and immunoblotting. Lane 1 = control; lane 2 = cuprizone treatment (CPZ); lane 3 = cuprizone and 4HQ (CPZ and 4HQ) treatment; lane 4 = 4HQ only. Results on the diagram are expressed as mean pixel densities ± SD; *$P < 0.05$ compared with control; ‡$P < 0.05$ compared with cuprizone group. Experiments were repeated three times and at least five mice were included in each group in all experiments. (**B**) Representative anti-poly(ADP-ribose) (PAR) immunohisto-chemistry image of corpus callosum in a cuprizone-treated mouse. Brown colour indicates strong poly(ADP-ribose) reactivity in the nucleus of an oligodendrocyte with condensed nuclei in active lesion (arrow). The insert indicates an apoptotic oligodendrocyte stained for carboanhydrase II as a marker for oligodendrocytes and DAPI, showing the fragmented nucleus (scale bar: 10 μm). (**C**) Representative confocal images of PARP activation in an oligodendrocyte. carbonic anhydrase II immunoreactivity (red), poly(ADP-ribose) immunoreactivity (green) and DAPI nuclear staining (blue) were presented individually and merged (left upper panel) (scale bar: 10 μm).

an effect that was attenuated by 4HQ (Fig. 6A). Besides elevating its expression, cuprizone induced nuclear translocation of AIF. In cuprizone-treated mice, numerous cells showing typical shape and arrangement of oligodendrocytes gave strong nuclear anti-AIF immunostaining in the midline and cingular part of the corpus callosum, which were prevented by the PARP inhibitor (Fig. 6B–D). In contrast, cuprizone did not induce caspase-dependent cell death, as revealed by the absence of procaspase-3 cleavage determined by immunoblotting and a fluorescent caspase-3 assay (data not shown). Taken together, these data indicate caspase-independent AIF-mediated cell death in the corpus callosum of cuprizone-fed mice, similar to that in multiple sclerosis, which could be attenuated by inhibition of PARP.

Cuprizone treatment activates Akt and mitogen-activated protein kinases in the corpus callosum, and is modulated by PARP inhibition

Three weeks of cuprizone feeding induced activation of the MAPKs, i.e. JNK, p38-MAPK and ERK ½ ($P < 0.01$, respectively) and Akt ($P < 0.05$) indicated by immunoblotting utilizing phosphorylation-specific primary antibodies (Fig. 7). 4HQ treatment attenuated cuprizone-induced phosphorylation of JNK and p38-MAPK ($P < 0.01$ and $P < 0.05$, respectively) but not of ERK1/2 (Fig. 7A and B). 4HQ alone did not affect phosphorylation of the MAPKs.

In contrast to the effect on MAPKs, 4HQ enhanced cuprizone-induced phosphorylation of Akt ($P < 0.05$). In addition, PARP inhibition alone also resulted in increased phosphorylation of Akt ($P < 0.05$) (Fig. 7C and D).

Discussion

In this article, we used cuprizone-induced demyelination as an animal model for oligodendrocyte depletion, as observed in multiple sclerosis, and its prevention by PARP inhibition. Demyelination and oligodendrocyte death are two of the general features of multiple sclerosis, which have even been suggested to be the primary events in lesion evolution, and may contribute to chronic inflammation through epitope spreading and axonal degeneration, which correlates with clinical disability (Naismith and Cross, 2005). Alternatively, oligodendrocyte injury and tissue destruction may be the consequence of the inflammatory process of multiple sclerosis (Smith and Lassmann, 2002; Lassmann et al., 2007). Irrespective of the primary trigger for oligodendrocyte death in multiple sclerosis, mitochondrial dysfunction with subsequent apoptotic cell death is a cardinal feature in at least a subset of acute and chronic multiple sclerosis lesions (Aboul-Enein et al., 2003; Mahad et al., 2008) and this feature is shared between the cuprizone model and multiple sclerosis.

Mitochondrial dysfunction with excessive reactive oxygen species production suggested by previous studies (Suzuki, 1969; Hemm et al., 1971; Ludwin, 1978; Pasquini et al., 2007; Turrens, 2003) could cause the PARP activation observed by us
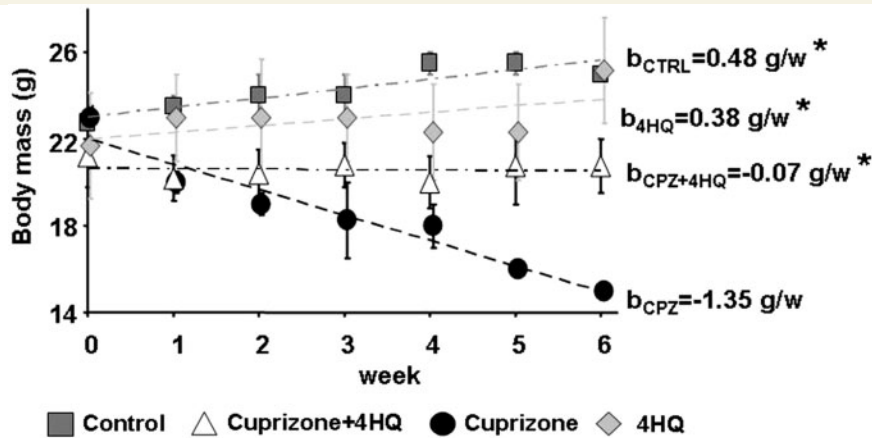
Figure 4 Effect of cuprizone and 4HQ treatment on body mass changes. Results are expressed as mean body mass ± SD of the 240 mice included in this study. Random intercept fixed slope linear model was used to determine weekly growth rates (b) indicated at the right edge of the figure; *$P < 0.001$ compared with the cuprizone (CPZ) group.

of degenerating oligodendrocytes in the cuprizone model and active pattern III multiple sclerosis lesions. Overactivation of PARP promotes cell death by ATP depletion in the cell and regulating the release of AIF from mitochondria (Yu *et al.,* 2002; Alano *et al.,* 2004). AIF then translocates to the nucleus, leading to chromatin condensation, large-scale DNA fragmentation (>50 kb) and cell death in a caspase-independent manner (Lorenzo and Susin, 2004; Jurewicz *et al.,* 2005). In fact, we observed nuclear translocation of AIF co-localized with poly(ADP-ribose) in several oligodendrocytes in both pattern III multiple sclerosis lesions and the cuprizone model. However, we were unable to detect caspase-3 activation in the corpus callosum of cuprizone-treated mice in agreement with previous findings (Copray *et al.,* 2005; Pasquini *et al.,* 2007).

Specificity and possible side-effects of a pharmacological agent are always an issue. However, 4HQ was reported to have a high potency for PARP-1 and no effects on enzymes other than PARP have been documented (Banasik *et al.,* 1992). Therefore, it seems likely that prevention of the weight loss, diminished demyelination and oligodendrocyte loss induced by cuprizone can be assigned to the PARP inhibitory effect of 4HQ.

JNK and p38-MAPK activation are considered to promote cell death (Xia *et al.,* 1995; Stariha and Kim, 2001; Ha *et al.,* 2002; Jurewicz *et al.,* 2003). Indeed, we observed that cuprizone increased phosphorylation of JNK and p38-MAPK in the corpus callosum, which was attenuated upon PARP inhibition. Cuprizone also induced ERK1/2 activation in the corpus callosum but it was not affected by the PARP inhibitor 4HQ, which can be explained by the notion that the MAPK/ERK kinase-ERK1/2 pathway is upstream to PARP activation (Tang *et al.,* 2002; Kauppinen *et al.,* 2006). Since ERK activation was found to promote oligodendrocyte survival (Cohen *et al.,* 1996; Yoon *et al.,* 1998), cuprizone-induced ERK activation may represent a protective mechanism against oligodendrocyte death. In conclusion, all effects of PARP inhibition on the MAPK pathways, i.e. suppressing JNK and p38 activation while not affecting ERK, could promote oligodendrocyte survival.

Cuprizone intoxication also resulted in Akt phosphorylation, which was further enhanced by co-administration of 4HQ. Furthermore, PARP inhibition alone caused phosphorylation of Akt in accordance with previous findings (Veres *et al.,* 2003; Tapodi *et al.,* 2005). Activation of Akt prevented neuronal apoptosis by inhibiting translocation of AIF to the nucleus (Kim *et al.,* 2007), protected oligodendrocytes against tumour necrosis factor-induced apoptosis (Pang *et al.,* 2007); and, by phosphorylating their respective upstream kinases, decreased activity of JNK and p38-MAPK (Park *et al.,* 2002; Barthwal *et al.,* 2003). Based on these data, our results may suggest that in response to cuprizone, the cytoprotective phosphatidylinositol-3 kinase/Akt pathway became activated, although it was insufficient to prevent oligodendrocyte death. Additional activation by PARP inhibition could be sufficient to protect oligodendrocytes against apoptosis, mediated partially by reduced activation of JNK and p38-MAPK and maintaining the integrity of the mitochondrial membrane systems preventing nuclear translocation of AIF.

In the cuprizone model of demyelination, the pathological changes are similar to pattern III lesions or lesions defined by Barnett and Prineas (Lucchinetti *et al.,* 2000; Barnett and Prineas, 2004). The earliest change in these lesions is wide-spread oligodendrocyte apoptosis associated with microglia activation in the proximity of dying oligodendrocytes, while signs of humoral and cellular immune responses are minor. Besides the pathological similarities, we observed identical patterns of at least two key molecular mechanisms, i.e. PARP activation and caspase-independent AIF-mediated apoptosis of oligodendrocytes in both pattern III multiple sclerosis lesions and cuprizone-induced demyelination. Based on these pathological and molecular observations, it could be assumed that the apoptosis of oligodendrocytes, at least in a subgroup of multiple sclerosis patients and in the cuprizone model, happens via similar pathways. Thus, inhibition of PARP may be similarly effective in multiple sclerosis and may have several important aspects. By blocking demyelination, PARP inhibition may reduce inflammation through preventing epitope spreading. Besides, it also has a direct effect on inflammation
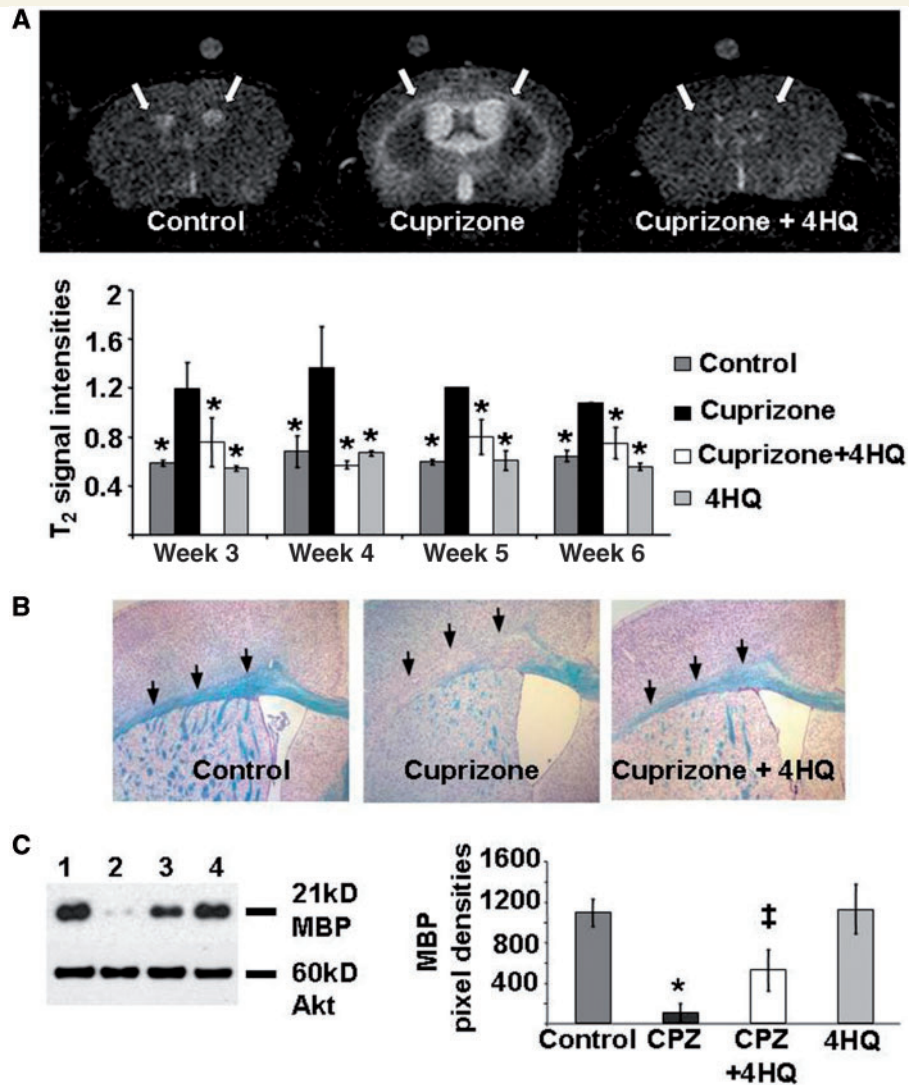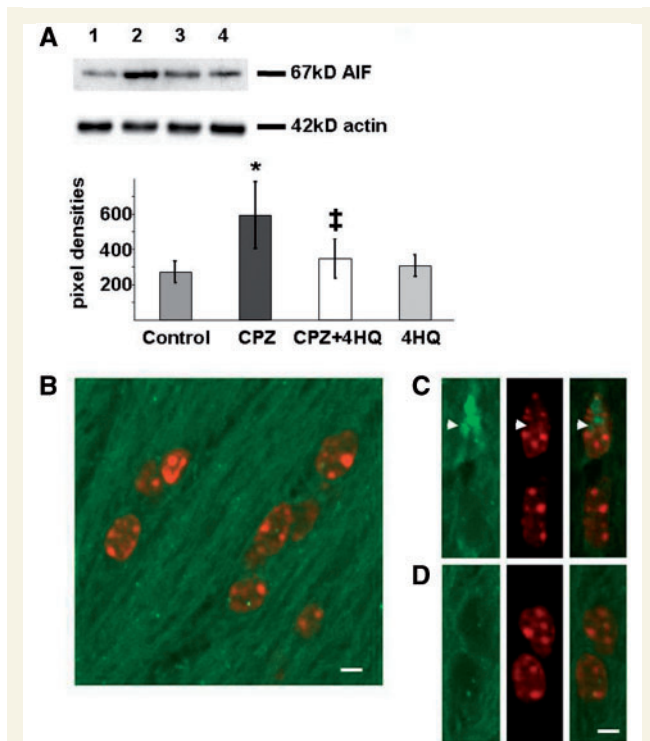
Figure 5 Effect of cuprizone and 4HQ treatment on demyelination in corpus callosum. (**A**) Representative T_2-weighted spin echo magnetic resonance images of brain coronal sections (upper panels) and quantification of T_2 intensity changes in the corpus callosum (lower panels) of mice treated for 4 weeks. Arrows indicate hyperintensities (suggesting demyelination) or hypointensity (intact myelin status) in corpus callosum. Data are expressed as normalized mean signal intensities ± SD. *$P < 0.001$ compared with the cuprizone (CPZ) group. Experiments were repeated three times and at least five mice were included in each group. (**B**) Representative histopathology images and quantification of myelin status in the corpus callosum (arrows) on brain coronal sections of mice treated for 5 weeks. Blue staining by luxol fast blue indicates intact myelin sheath. Experiments were repeated at least three times and at least five mice were included in each group. (**C**) MBP expression in the dissected corpus callosum of mice treated for 5 weeks was detected by immunoblotting utilizing an anti-MBP antibody. Even protein loadings were confirmed by an anti-Akt antibody and immunoblotting. Representative immunoblots (left panel) from three experiments with similar results and densitometric evaluation (right panel) are shown. At least five mice were included in each group. Lane 1 = control; lane 2 = cuprizone (CPZ) treatment; lane 3 = cuprizone+4HQ (CPZ+4HQ) treatment; lane 4 = 4HQ only. Results on the diagram are expressed as the mean pixel densities ± SD; *$P < 0.01$ compared with control; ‡$P < 0.05$ compared with the cuprizone group.

indicated by a reduction in the clinical signs of experimental auto-immune encephalomyelitis (Scott *et al.*, 2004). Inhibiting PARP may thus influence degenerative and autoimmune inflammatory processes in multiple sclerosis and provide an effective therapy targeting two basic mechanisms at the same time. Recently, plasma exchange has been shown to be highly efficient in patients with antibody-med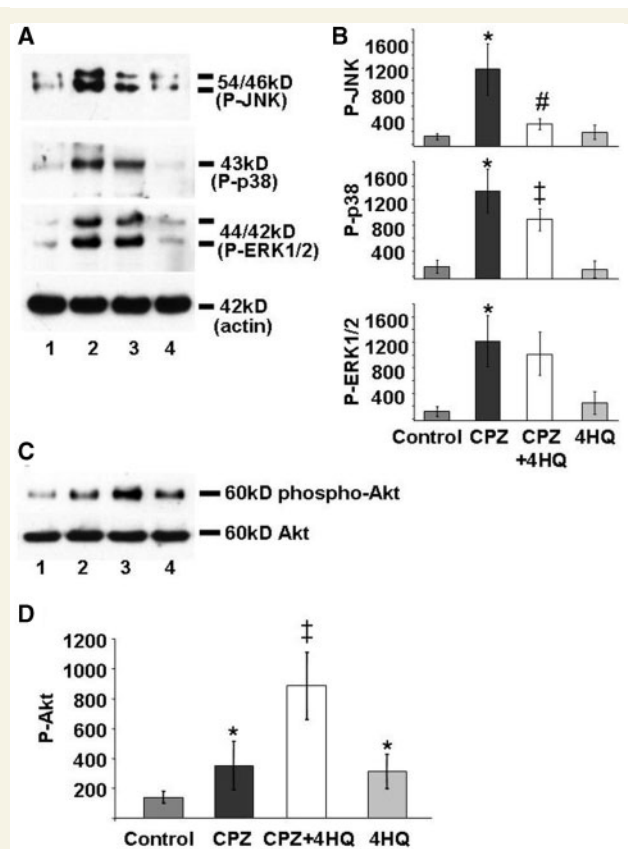iated pattern II lesions indicating the importance of mechanism-specific treatment strategies (Keegan *et al.*, 2005). Similarly, PARP-inhibitors may be effective in patients with pattern III lesions characterized by primary oligodendrocyte death.

In summary, our data indicate that oligodendrocyte death occurs via very similar mitochondrial pathomechanisms in the cuprizone model and pattern III multiple sclerosis lesions.

Figure 6 Effect of cuprizone and 4HQ treatment on the expression and nuclear translocation of AIF in the corpus callosum. (**A**) Expression of AIF in the dissected corpus callosum of mice treated for 3 weeks was detected by immunoblotting. Representative immunoblots from three experiments (at least five mice in each group) and densitometric evaluations are shown. Even protein loadings were confirmed by anti-actin antibody and immunoblotting. Lane 1 = control; lane 2 = cuprizone (CPZ) treatment; lane 3 = cuprizone and 4HQ (CPZ+4HQ) treatment; lane 4 = 4HQ treatment. Results on diagram are expressed as the mean pixel densities ± SD; *$P < 0.05$ compared with control; ‡$P < 0.05$ compared with the cuprizone group. (**B–D**) For demonstration of its nuclear translocation, AIF (green) immunohistochemisty with DAPI nuclear counterstaining (red) was performed, and confocal microscopy images were taken from representative areas of the midline of the corpus callosum of mice treated for 3 weeks. Photomicrographs were taken using a ×60 oil immersion objective. Experiments were repeated at least three times (at least five mice in each group) with identical results. (**B**) Representative merged image of untreated control mice (scale bar: 10 μm). (**C** and **D**) Representative images of the green channel (left panels), the red channel (middle panel) and merged channels (right panel) of cuprizone (**C**) and cuprizone + 4HQ (**D**) treated mice. Arrowheads indicate a cell where nuclear translocation of AIF occurred (scale bar: 10 μm). Experiments were repeated three times and at least five mice were included in each group in all experiments.

Figure 7 Effect of cuprizone and 4HQ treatment on the phosphorylation state of mitogen-activated protein kinases and Akt in the corpus callosum. MAPK (**A** and **B**) and Akt (**C** and **D**) phosphorylation in the dissected corpus callosum of mice treated for 3 weeks was detected by immunoblotting utilizing phosphorylation-specific antibodies (P-Thr^{180}/Tyr^{182}-p38-MAPK, P-Thr^{183}/Tyr^{185} -JNK, P-Thr^{183}/Tyr^{185}- ERK1/2, P-Ser^{473} Akt). Even protein loadings were confirmed by anti-actin (**A**) and anti-Akt (**C**) antibodies and immunoblotting. Representative immunoblots (**A** and **C**) from three experiments (at least five mice in each group) and densitometric evaluations (**B** and **D**) are shown. (**A** and **B**) Lane 1 = control; lane 2 = cuprizone (CPZ) treatment; lane 3 = cuprizone and 4HQ (CPZ+4HQ) treatment; lane 4 = 4HQ treatment. Results on the diagram are expressed as mean pixel densities ± SD; *$P < 0.01$ compared with control; #$P < 0.01$ compared with the cuprizone group; ‡$P < 0.05$ compared with cuprizone group. (**C** and **D**) Lane 1 = control; lane 2 = cuprizone (CPZ) treatment; lane 3 = cuprizone and 4HQ (CPZ+4HQ) treatment; lane 4 = 4HQ treatment. Results on the diagram are expressed as the mean pixel densities ± SD; *$P < 0.05$ compared with control; ‡$P < 0.05$ compared with the cuprizone group.

Inhibition of PARP effectively attenuated oligodendrocyte depletion and protected against experimental demyelination mediated through a caspase-independent pathway involving nuclear translocation of AIF. Considering that PARP inhibition was also highly effective in experimental autoimmune encephalomyelitis, the autoimmune inflammatory model of multiple sclerosis (Scott *et al.*, 2004), it may provide a therapeutic approach protecting against two basic processes in multiple sclerosis, inflammation and demyelination. Moreover, it may target all subtypes of multiple sclerosis either by preventing oligodendrocyte death, a key event in the formation of all new lesions or additionally, by targeting inflammation.

Acknowledgements

Funding

References

Aboul-Enein F, Rauschka H, Kornek B, Stadelmann C, Stefferl A, Brück W, et al. Preferential loss of myelin-associated glycoprotein reflects hypoxia-like white matter damage in stroke and inflammatory brain diseases. J Neuropathol Exp Neurol 2003; 62: 25–33.

Alano CC, Ying W, Swanson RA. Poly(ADP-ribose) polymerase-1-mediated cell death in astrocytes requires NAD+ depletion and mitochondrial permeability transition. J Biol Chem 2004; 279: 18895–902.

Banasik M, Komura H, Shimoyama M, Ueda K. Specific inhibitors of poly(ADP-ribose) synthase and mono(ADP-ribosyl) transferase. J Biol Chem 1992; 267: 1569–75.

Barnett MH, Prineas JW. Relapsing and remitting multiple sclerosis: pathology of the newly forming lesion. Ann Neurol 2004; 55: 458–68.

Barthwal MK, Sathyanarayana P, Kundu CN, Rana B, Pradeep A, Sharma C, et al. Negative regulation of mixed lineage kinase 3 by protein kinase B/AKT leads to cell survival. J Biol Chem 2003; 278: 3897–902.

Bauer J, Elger CE, Volkmar HH, Schramm J, Urbach H, Lassmann H, et al. Astrocytes are a specific immunological target in Rasmussen's encephalitis. Ann Neurol 2007; 62: 67–80.

Cohen RI, Marmur R, Norton WT, Mehler MF, Kessler JA. Nerve growth factor and neutrotrophin-3 differentially regulate the proliferation and survival of developing rat brain oligodendrocytes. J Neurosci 1996; 16: 6433–42.

Copray JCVM, Küst BM, Mantingh-Otter I, Boddeke HWGM. p75NTR independent oligodendrocyte death in cuprizone-induced demyelination in C57BL/6 mice. Neuropathol Appl Neurol 2005; 31: 600–9.

Endres M, Wang ZQ, Namura S, Waeber C, Moskowitz MA. Ischemic brain injury is mediated by the activation of poly(ADP-ribose) polymerase. J Cereb Blood Flow Metab 1997; 17: 1143–51.

Frohman EM, Racke MK, Raine CS. Multiple sclerosis–the plaque and its pathogenesis. N Engl J Med 2006; 354: 942–55.

Ha HC, Hester LD, Snyder H. Poly(ADP-ribose) polymerase-1 dependence of stress-induced transcription factors and associated gene expression in glia. Proc Natl Acad Sci USA 2002; 99: 3270–5.

Hemm RD, Carlton WW, Wesler JR. Ultrastructural changes of cuprizone encephalopathy in mice. Toxicol Appl Pharm 1971; 28: 869–82.

Hiremath MM, Saito Y, Knapp GW, Ting JP-Y, Suzuki K, Matsushima GK. Microglial/macrophage accumulation during cuprizone-induced demyelination in C57BL/6 mice. J Neuroimmunol 1998; 92: 38–49.

Jurewicz A, Matysiak M, Tybor K, Selmaj K. TNF-induced death of adult human oligodendrocytes is mediated by the c-jun NH2-terminal kinase-3. Brain 2003; 126: 1358–70.

Jurewicz A, Matysiak M, Tybor K, Kilianek L, Raine CS, Selmaj K. Tumour necrosis factor-induced death of adult human oligodendrocytes is mediated by apoptosis inducing factor. Brain 2005; 128: 2675–88.

Kalman B, Laitinen K, Komoly S. The involvement of mitochondria in the pathogenesis of multiple sclerosis. J Neuroimmunol 2007; 188: 1–12.

Kauppinen TM, Chan WY, Suh SW, Wiggins AK, Huang EJ, Swanson RA. Direct phosphorylation and regulation of poly(ADP-ribose) polymerase-1 by extracellular signal-regulated kinases 1/2. Proc Natl Acad Sci USA 2006; 103: 7136–41.

Kauppinen TM, Swanson RA. The role of poly(ADP-ribose) polymerase-1 in CNS disease. Neuroscience 2007; 145: 1267–72.

Keegan M, König F, McClelland R, Brück W, Morales Y, Bitsch A, et al. Relation between humoral pathological changes in multiple sclerosis and response to therapeutic plasma exchange. Lancet 2005; 366: 579–82.

Kim NH, Kim K, Park WS, Son HS, Bae Y. PKB/Akt inhibits ceramide-induced apoptosis in neuroblastoma cells by blocking apoptosis-inducing factor (AIF) translocation. J Cell Biochem 2007; 102: 1160–70.

Kutzelnigg A, Lucchinetti CF, Stadelmann C, Brück W, Rauschka H, Bergmann M, et al. Cortical demyelination and diffuse white matter injury in multiple sclerosis. Brain 2005; 128: 2705–12.

Lassmann H, Brück W, Lucchinetti C. The immunopathology of multiple sclerosis: an overview. Brain Pathol 2007; 17: 210–8.

Lorenzo HK, Susin SA. Mitochondrial effectors in caspase-independent cell death. FEBS Lett 2004; 557: 14–20.

Lucchinetti C, Brück W, Parisi J, Scheithauer B, Rodriguez M, Lassmann H. Heterogeneity of multiple sclerosis lesions: implications for the pathogenesis of demyelination. Ann Neurol 2000; 47: 707–17.

Ludwin SK. Central nervous system demyelination and remyelination in the mouse: an ultrastructural study of cuprizone toxicity. Lab Invest 1978; 39: 597–612.

Mahad D, Ziabreva I, Lassmann H, Turnbull D. Mitochondrial defects in acute multiple sclerosis lesions. Brain 2008; 131: 1722–35.

Mandir AS, Poitras FM, Berliner AR, Herring WJ, Guastella DB, Feldman A, et al. NMDA but not non-NMDA excitotoxicity is mediated by poly(ADP-ribose) polymerase. J Neurosci 2000; 20: 8005–11.

Marburg O. Die sogenannte ''akute Multiple Sklerose''. Jahrb Psychiatrie 1906; 27: 211–312.

Marik C, Felts P, Bauer J, Lassmann H, Smith KJ. Lesion genesis in a subset of patients with multiple sclerosis: a role for innate immunity? Brain 2007; 130: 2800–15.

Matsushima GK, Morell P. The neurotoxicant, cuprizone, as a model to study demyelination and remyelination in the central nervous system. Brain Pathol 2001; 11: 107–16.

Merkler D, Boretius S, Stadelmann C, Ernsting T, Michaelis T, Frahm J, et al. Multicontrast MRI of remyelination in the central nervous system. NMR Biomed 2005; 6: 395–403.

Naismith RT, Cross AH. Multiple sclerosis and black holes: connecting the pixels. Arch Neurol 2005; 62: 1666–8.

Noseworthy JH, Lucchinetti C, Rodriguez M, Weinshenker B. Multiple sclerosis. N Engl J Med 2000; 343: 938–52.

Oliver FJ, Ménissier-de Murcia J, Nacci C, Decker P, Andriantsitohaina R, Muller S, et al. Resistance to endotoxic shock as a consequence of defective NF-kappaB activation in poly (ADP-ribose) polymerase-1 deficient mice. EMBO J 1999; 18: 4446–54.

Pang Y, Zheng B, Fan LW, Rhodes PG, Cai Z. IGF-1 protects oligodendrocyte progenitors against TNFα-induced damage by activation of PI3K/Akt and interruption of the mitochondrial apoptotic pathway. Glia 2007; 55: 1099–107.

Park HS, Kim M-S, Huh S-H, Park J, Chung J, Kang SS, et al. Akt (protein kinase B) negatively regulates SEK1 by means of protein phosphorylation. J Biol Chem 2002; 277: 2573–8.

Pasquini LA, Calatayud CA, Bertone Uña AL, Millet V, Pasquini JM, Soto EF. The neurotoxic effect of cuprizone on oligodendrocytes depends on the presence of pro-inflammatory cytokines secreted by microglia. Neurochem Res 2007; 32: 279–92.

Remington LT, Babcock AA, Zehntner SP, Owens T. Microglial recruitment, activation, and proliferation in response to primary demyelination. Am J Pathol 2007; 170: 1713–24.

Scott GS, Kean RB, Mikheeva T, Fabis MJ, Mabley JG, Szabó C, et al. The therapeutic effects of PJ34 [N-(6-Oxo-5,6-dihydrophenanthridin-2-yl)-N,N-dimethylacetamide.HCl], a selective inhibitor of poly (ADP-ribose) polymerase, in experimental allergic encephalomyelitis are associated with immunomodulation. J Pharmacol Exp Ther 2004; 310: 1053–61.

Sidman RL. Atlas of the mouse brain and spinal cord. Cambridge: Harvard University Press; 1971.

Smith K, Lassmann H. The role of nitric oxide in multiple sclerosis. Lancet Neurol 2002; 1: 202–41.

Stariha RL, Kim SU. Mitogen-activated protein kinase signalling in oligodendrocytes: a comparison of primary cultures and CG-4. Int J Devl Neurosci 2001; 19: 427–37.

Suzuki K. Giant hepatic mitochondria: production in mice fed with cuprizone. Science 1969; 163: 81–2.

Tang D, Wu D, Hirao A, Lahti JM, Liu L, Mazza B, et al. ERK activation mediates cell cycle arrest and apoptosis after DNA damage independently of p53. J Biol Chem 2002; 277: 12710–7.

Tapodi A, Debreceni B, Hanto K, Bognar Z, Wittmann I, Gallyas F Jr, et al. Pivotal role of Akt activation in mitochondrial protection and cell survival by poly(ADP-ribose)polymerase-1 inhibition in oxidative stress. J Biol Chem 2005; 280: 35767–75.

Turrens JF. Mitochondrial formation of reactive oxygen species. J Physiol 2003; 552: 335–44.

Veres B, Gallyas F Jr, Varbiro G, Berente Z, Osz E, Szekeres G, et al. Decrease of the inflammatory response and induction of the Akt/protien kinase B pathway by poly-(ADP-ribose) polymerase 1 inhibitor in endotoxin-induced septic shock. Biochem Pharmacol 2003; 65: 1373–82.

Veres B, Radnai B, Gallyas F Jr, Varbiro G, Berente Z, Osz E, et al. Regulation of kinase cascades and transcription factors by a poly(ADP-ribose) polymerase-1 inhibitor, 4-hydroxyquinazoline, in lipopolysaccharide-induced inflammation in mice. J Pharmacol Exp Ther 2004; 310: 247–55.

Xia Z, Dickens M, Raingeaud J, Davis RJ, Greenberg ME. Opposing effects of ERK and JNK-p38 MAP kinases on apoptosis. Science 1995; 207: 1326–31.

Xu Y, Huang S, Liu ZG, Han J. Poly(ADP-ribose) polymerase-1 signaling to mitochondria in necrotic cell death requires RIP1/TRAF2-mediated JNK1 activation. J Biol Chem 2006; 281: 8788–95.

Yoon SO, Casaccia-Bonnefil P, Carter B, Chao MV. Competitive signaling between TrkA and p75 nerve growth factor receptors determines cell survival. J Neurosci 1998; 18: 3273–81.

Yu SW, Wang H, Poitras MF, Coombs C, Bowers WJ, Federoff HJ, et al. Mediation of poly(ADP-ribose) polymerase-1-dependent cell death by apoptosis inducing factor. Science 2002; 297: 259–63.